N94-34977

Paper Proposed for Presentation to the
Workshop on Physics of Forced Unsteady Separation
to be held at
NASA Ames Research Center April 17–19, 1990

COMPUTATION OF UNSTEADY FLOWS OVER AIRFOILS

J. A. Ekaterinaris
Navy–NASA Joint Inst. of Aeronautics
Dept. of Aeronautics and Astronautics
Naval Postgraduate School
NASA–Ames Research Center
Mail Stop 258-1
Moffett Field, CA 94035

M. F. Platzer
Navy–NASA Joint Inst. of Aeronautics
Dept. of Aeronautics and Astronautics
Naval Postgraduate School
Monterey, CA 93943

SUMMARY

Two methods are described for calculating unsteady flows over rapidly pitching airfoils. The first method is based on an interactive scheme in which the inviscid flow is obtained by a panel method. The boundary layer flow is computed by an interactive method that makes use of the Hilbert integral to couple the solutions of the inviscid and viscous flow equations. The second method is based on the solution of the compressible Navier–Stokes equations. The solution of these equations is obtained with an approximately factorized numerical algorithm, and with single block or multiple grids which enable grid embedding to enhance the resolution at isolated flow regions. In addition, the attached flow region can be computed by the numerical solution of compressible boundary layer equations. Unsteady pressure distributions obtained with both methods are compared with available experimental data.

ABSTRACT

The present paper addresses the prediction of unsteady airfoil boundary layer flows by two methods. These two methods are briefly described in the following section. The first is based on the extension of the steady interactive boundary–layer method of [1] and the second on the Navier–Stokes method of [2].

PRECEDING PAGE BLANK NOT FILMED

1.1 Viscous–Inviscid Interaction Method: The interactive method for steady high Reynolds number incompressible flows is described in [1] and [3], respectively, and makes use of an inverse boundary–layer method coupled to a panel method with an interactive formula suggested by Veldman [4]. The extension of this method to unsteady incompressible flows, again makes use of a panel method [5], which is similar to that of Hess and Smith [6]. This method utilizes the procedure of Basu and Hancock [7] to model the wake. The wake is represented by a series of free vortices shed from the trailing edge in response to incidence changes so that the total vorticity in the field is conserved. The airfoil's lift response then is obtained by subdividing the incidence history into sufficiently small time steps and computing the source and vorticity distributions for each time step. The unsteady interactive method is described in full detail in Refs. 5 and 8.

The unsteady boundary–layer equations are expressed in terms of an eddy viscosity, ϵ_m, so that continuity and momentum equations

$$\frac{\partial u}{\partial x} + \frac{\partial v}{\partial y} = 0 \tag{1}$$

$$\frac{\partial u}{\partial t} + u\frac{\partial u}{\partial x} + v\frac{\partial u}{\partial y} = \frac{\partial U_e}{\partial t} + U_e\frac{\partial U_e}{\partial x} + \frac{\partial}{\partial y}\left[(\nu + \epsilon_m)\frac{\partial u}{\partial y}\right] \tag{2}$$

are solved subject to the boundary conditions

$$y = 0, \quad u = v = 0; \qquad y \longrightarrow \infty, \quad u \longrightarrow U_e(x,t) \tag{3}$$

on the airfoil and with y = 0 denoting the dividing streamline that separates the upper and lower parts of the inviscid flow in the wake, subject to the following conditions

$$y \longrightarrow \pm\infty, \qquad u \longrightarrow U_e(x,t); \qquad y = 0, \qquad v = 0 \tag{4}$$

with $U_e(x,t)$ given by $U_e = U_e^o + \delta U_e(x,t)$. The eddy viscosity formulation of Cebeci and Smith [9] is used with special emphasis on the transitional region.

1.2 Navier–Stokes Methods : The Navier -Stokes method is briefly described in this paragraph. The full, unsteady, two–dimensional, compressible Navier–Stokes equations were solved. In a curvilinear coordinate system ξ, η the governing equations are:

$$\frac{\partial \hat{\mathbf{q}}}{\partial t} + \frac{\partial \hat{\mathbf{F}}}{\partial \xi} + \frac{\partial \hat{\mathbf{G}}}{\partial \eta} = \frac{1}{Re}\left(\frac{\partial \hat{\mathbf{R}}}{\partial \xi} + \frac{\partial \hat{\mathbf{S}}}{\partial \eta}\right) \tag{5}$$

where $\hat{\mathbf{q}}$ is the conservative variable vector $\mathbf{q} = (\rho, \rho u, \rho v, e)^T$, and $\hat{\mathbf{F}}$, $\hat{\mathbf{G}}$ are the nonlinear inviscid terms, and $\hat{\mathbf{R}}, \hat{\mathbf{S}}$ are the viscous terms.

The integration is performed with the finite difference factored Beam–Warming algorithm [10]. The approximately factorized form of the algorithm is:

$$\begin{aligned}&\left[I + (\Delta t/2)\left(\delta_\xi A^n_{j,k} + (D_{impl})_\xi\right)\right]\times \\ &\left[I + (\Delta t/2)\left(\delta_\eta B^n_{j,k} + (D_{impl})_\eta\right)\right]\Delta\mathbf{q}^n_{j,k} = (RHS)^n\end{aligned} \tag{6}$$

where

$$(RHS)^n = \Delta t(-\delta_\xi \mathbf{F}^n_{j,k} - \delta_\eta \mathbf{G}^n_{j,k} + \delta_\xi \mathbf{R}^n_{j,k} + \delta_\eta \mathbf{S}^n_{j,k} - \epsilon_{expl}(D_{expl})^n_{j,k}) \tag{7}$$

Solutions with embedded grid which provide enhanced grid resolution at isolated flow regions are possible. Thus, high grid resolution can be provited at critical flow regions, such as the leading edge region, where supersonic flow conditions and possible shock formation may occur even at moderate free stream subsonic speeds ($M = 0.45 - 0.50$) as the angle of attack increases. The option of solving the attached flow region with the compressible boundary–layer equations on an embedded grid is also provided. The boundary–layer equations for a generalized coordinates system [11] are:

continuity

$$\frac{\partial}{\partial t}\left(\frac{\rho}{J}\right) + \frac{\partial}{\partial \xi}\left(\frac{\rho U}{J}\right) + \frac{\partial}{\partial \eta}\left(\frac{\rho V}{J}\right) = 0 \tag{8}$$

ξ momentum

$$\rho\frac{\partial u}{\partial t} + \rho U\frac{\partial u}{\partial \xi} + \rho V\frac{\partial v}{\partial \eta} + \left(\xi_x\frac{\partial p}{\partial \xi} + \eta_x\frac{\partial p}{\partial \eta}\right) = J\frac{\partial}{\partial \xi}\left[\tau_{xx}\xi_x + \tau_{xy}\xi_y\right] + J\frac{\partial}{\partial \eta}\left[\tau_{xx}\eta_x + \tau_{yx}\eta_y\right] \tag{9}$$

normal momentum

$$\frac{\partial p}{\partial \eta} = 0 \tag{10}$$

energy

$$\begin{aligned}&\rho\frac{\partial H}{\partial t} - \frac{\partial p}{\partial t} + \rho u\frac{\partial H}{\partial \xi} + \rho v\frac{\partial H}{\partial \eta} = \\ &J\frac{\partial}{\partial \xi}\left\{\xi_x[\tau_{xx}u + \tau_{xy}v + K(\frac{\partial a^2}{\partial x})] + \xi_y[\tau_{xy}u + \tau_{yy}v + K(\frac{\partial a^2}{\partial y})]\right\} + \\ &J\frac{\partial}{\partial \eta}\left\{\eta_x[\tau_{xx}u + \tau_{xy}v + K(\frac{\partial a^2}{\partial x})] + \eta_y[\tau_{xy}u + \tau_{yy}v + K(\frac{\partial a^2}{\partial y})]\right\}\end{aligned} \tag{11}$$

Here $H = \frac{e+p}{\rho}$ is the enthalpy per unit volume, and the other quantities have the same definitions as before. Eqs. 8–11 are supplemented by the equation of state,

$$\frac{\rho}{\rho_\infty} = \frac{pT_\infty}{Tp_\infty} \tag{12}$$

or

$$\frac{T}{T_\infty} = \frac{(\gamma-1)}{a_\infty^2}[H - \frac{u^2+v^2}{2}] \tag{13}$$

Viscous or inviscid solutions can be obtained for the global grid by marching in time from an initial condition. Steady solutions are obtained by marching in time from free stream initial conditions until convergence to the steady–state. Similarly, unsteady flows are computed by marching in time from a steady flow initial condition. After the global grid solution is computed the boundary layer equations can be solved in the secondary grid using as initial condition at the inflow the velocity profile obtained by the viscous flow solution. Boundary conditions at the edge of the boundary layer domain are provided by the pressure and velocity distribution of a viscous or inviscid global flow solution for the outer region. Grid refinement is applied for the boundary–layer calculation and the values of the flow parameters at the extra boundary points are obtained by simple interpolation of the flow variables obtained from the viscous solution. For unsteady calculations the boundary layer equations are solved at each time step.

2.0 RESULTS AND DISCUSSION

The unsteady flow calculations for the NACA–0012 airfoil subject to ramp–type motion, as described in detail in [12], were performed by using both interactive and Navier–Stokes methods for a Reynolds number of 2.7×10^6 and for a non–dimensional pitch rate k defined by $k = \dot{\alpha}c/2U_\infty = 0.0127$. The airfoil chord was 10.16 cm, the pitch rate 1280 degrees/sec, pitching from 0^o to 15.54^o, at a free-stream Mach number of M = 0.3. The experimental data include upper and lower surface pressure distributions for incidence angles of 2.9, 5.8, 8.9, 11.7 and 15.5 degrees.

Figures 1 and 2 compare measured and calculated distributions of pressure coefficients for incidence angles of 2.9, 5.8, 8.9, 11.7 and 15.5 degrees, with Figure 1 showing the predictions of the interactive method and Figure 2 those of the Navier–Stokes method. In both methods, the flow was assumed to be fully turbulent due to the lack of experimental data about the location of transition, and the ramp change in the angle of attack was assumed to be given by

$$\alpha(t) = -\frac{2\alpha_{max}}{T^3}t^3 + \frac{3\alpha_{max}}{T^2}t^2 \tag{14}$$

where T is the nondimensional time required to complete the ramp motion from 0^o to α_{max}. It is useful to point out that while the interactive method is based on the assumption of incompressible flow, the Navier–Stokes method is for a compressible flow. Calculations performed with the Navier–Stokes equations for a Mach number of 0.2 and 0.3, however, showed no effect of compressibility on the results.

Figures 1 and 2 show that the predictions of both methods are in good agreement with the experimental data,although the Navier–Stokes computations slightly underpredict the suction peaks at the lower incidence. Figures 3 and 4 present a comparison between the velocity profiles computed by both methods at two chordwise locations corresponding to $x/c = 0.5$ and $x/c = 0.9$ at several angles of incidence. While there is reasonably good agreement at low incidences, the two profiles begin to deviate significantly at higher incidences. Figure 4e shows, however, that both procedures predict the onset of flow reversal at $\alpha = 15.5^o$ for $x/c = 0.9$. Unfortunately, there is no experimental data available to verify this prediction and to assess the accuracy of the two methods.

3.0 CONCLUSIONS

Two methods are described and applied to study the effects of low Reynolds number and flow unsteadiness on blade boundary layers. The first is based on an interactive boundary layer scheme in which the inviscid flow is computed by a panel method and the boundary layer flow by an inverse method that makes use of the Hilbert integral to couple the solutions of the inviscid and viscous flow equations. The second method is based on the solution of the compressible Navier–Stokes equations which employs an embedded grid technique for accurate boundary layer calculations with small computational cost. Calculated results obtained with both methods for a NACA–0012 airfoil subject to a ramp type motion at relatively high Reynolds number also indicate good agreement with experimental data. These results suggest that unsteady blade boundary layers can be computed accurately with either method provided the location of transition is computed interactively with the e^n–method and the transitional region is modelled properly. Future work will be directed at the systematic study of the effect of Reynolds number, transition modeling, reduced frequency and the effect of the airfoil leading edge geometry. In addition upwinding and TVD schemes will be used to enable accurate capturing of possible shock formation at the leading edge.

Acknowledgment: This work was supported by the Naval Air Systems Command, and NASA Ames Research Center.

References

[1] Cebeci, T., Clark, R. W., Chang, K. C., Halsey, N. D., and Lee, K., "Airfoils with Separation and the Resulting Wakes," *J. Fluid Mech.*, No. 163, pp. 323–347, 1986.

[2] Ekaterinaris, J. A., "Compressible Studies on Dynamic Stall," AIAA Paper 89-0024, 27th Aerospace Sciences Meeting, Reno NV, Jan. 1989.

[3] Cebeci, T., "Essential Ingredients of a Method for Low Reynolds Number Airfoils," To be published in the AIAA journal 1989.

[4] Veldman, A. E. P., "New Quasi–Simultaneous Method to Calculate Interactively Boundary Layers," *AIAA Journal,*, No. 19, 1981, p. 769.

[5] Teng, N. H., "The Development of a Computer Code (U2DIIF) for the Numerical Solution of Unsteady, Inviscid and Incompressible Flow over an Airfoil," M.S. Thesis, Naval Postgraduate School, Montery CA, 1987.

[6] Hess, J. L., and Smith, A. M. O., "Calculation of Potential Flow about Arbitrary Bodies," *Progress in Aeronautical Sciences*, Pergamon Press, Oxford, Vol. 8, 1966, pp 1–138.

[7] Basu, B. C., and Hancock, G. J. "The Unsteady Motion of a Two–Dimensional Airfoil in Incompressible Inviscid Flow," *Journal of Fluid Mech.*, Vol. 87, 1987, pp. 157–168.

[8] Jang , H. M., "A Viscous–Inviscid Interactive Method for Unsteady Flow," *Ph.D. Thesis, University of Michigan*, Ann Arbor, Michigan 1989.

[9] Cebeci, T, and Smith, A. M. O., "Analysis of Turbulent Boundary Layers," *Academic Press* , New York, 1974.

[10] Beam, R. M. and Warming, R. F., "An Implicit Factored Scheme for the Compressible Navier–Stokes Equations," *AIAA Journal*, Vol. 16, No. 4, April 1978, pp. 393–402.

[11] Steger, J. L, VanDalsem, W. R., Panaras, A. G., and Rao, K. V., "A Formulation for the Boundary–Layer Equations In General Coordinates," NASA Technical Memorandum 100079, June 1988.

[12] Landon, R. H., "NACA 0012 Oscillatory and Transient Pitching," AGARD Report No. 702, 1981.

Figure Captions

Figure 1. Pressure Coefficient at $\alpha = 2.9^o, 5.8^o, 8.9^o, 11.7^o, 15.5^o$ predicted by the viscous–inviscid interaction method. ($Re = 2.7 \times 10^6, k = 0.0127$)

Figure 2. Pressure Coefficient at $\alpha = 2.9^o, 5.8^o, 8.9^o, 11.7^o, 15.5^o$ predicted by the Navier–Stokes solution. ($Re = 2.7 \times 10^6, k = 0.0127$)

Figure 3. Comparison of the boundary–layer profiles computed with both methods, at $\alpha = 2.9^o, 5.8^o, 8.9^o, 11.7^o, 15.5^o$ for the 50% chord. ($Re = 2.7 \times 10^6, k = 0.0127$)

Figure 4. Comparison of the boundary–layer profiles computed with both methods, at $\alpha = 2.9^o, 5.8^o, 8.9^o, 11.7^o, 15.5^o$ for the 90% chord. ($Re = 2.7 \times 10^6, k = 0.0127$)

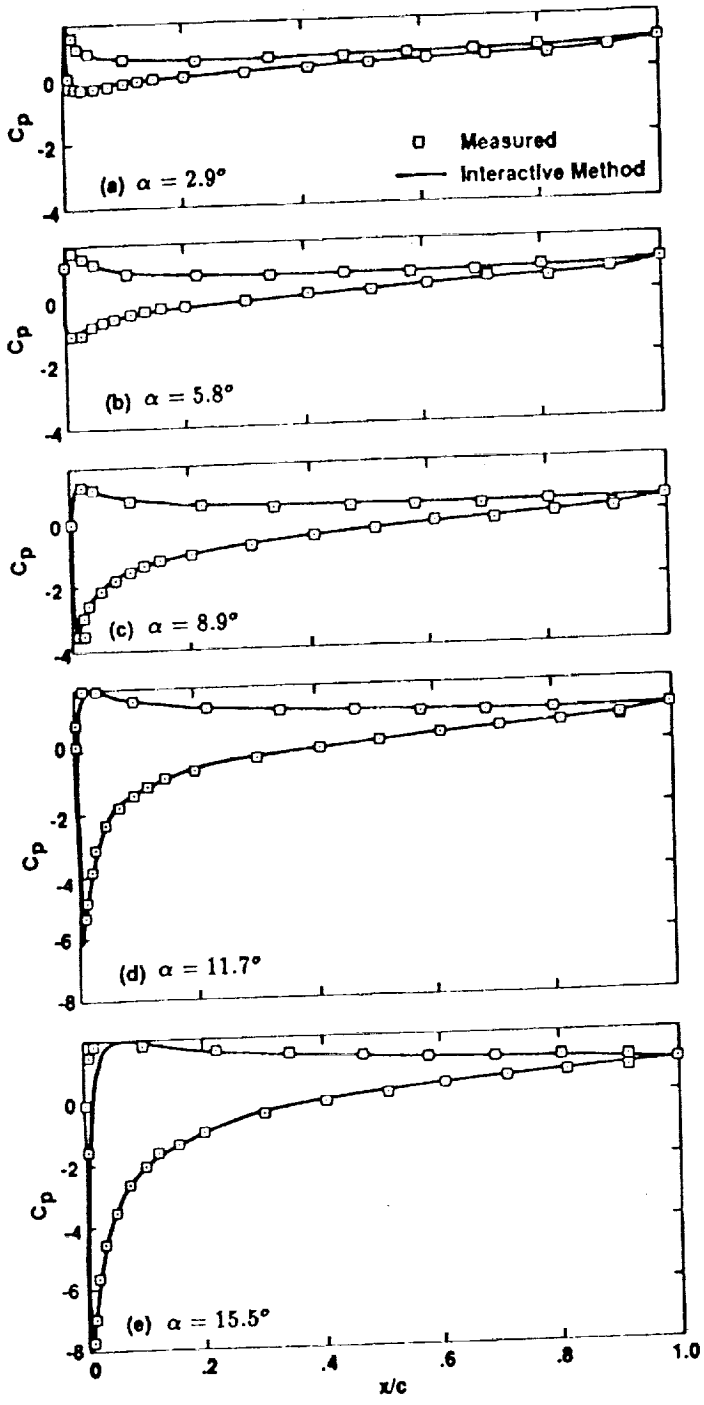

Figure 1 Pressure coefficient distributions predicted by the interactive method: ($Re = 2.7 \times 10^6, k = 0.0127$).

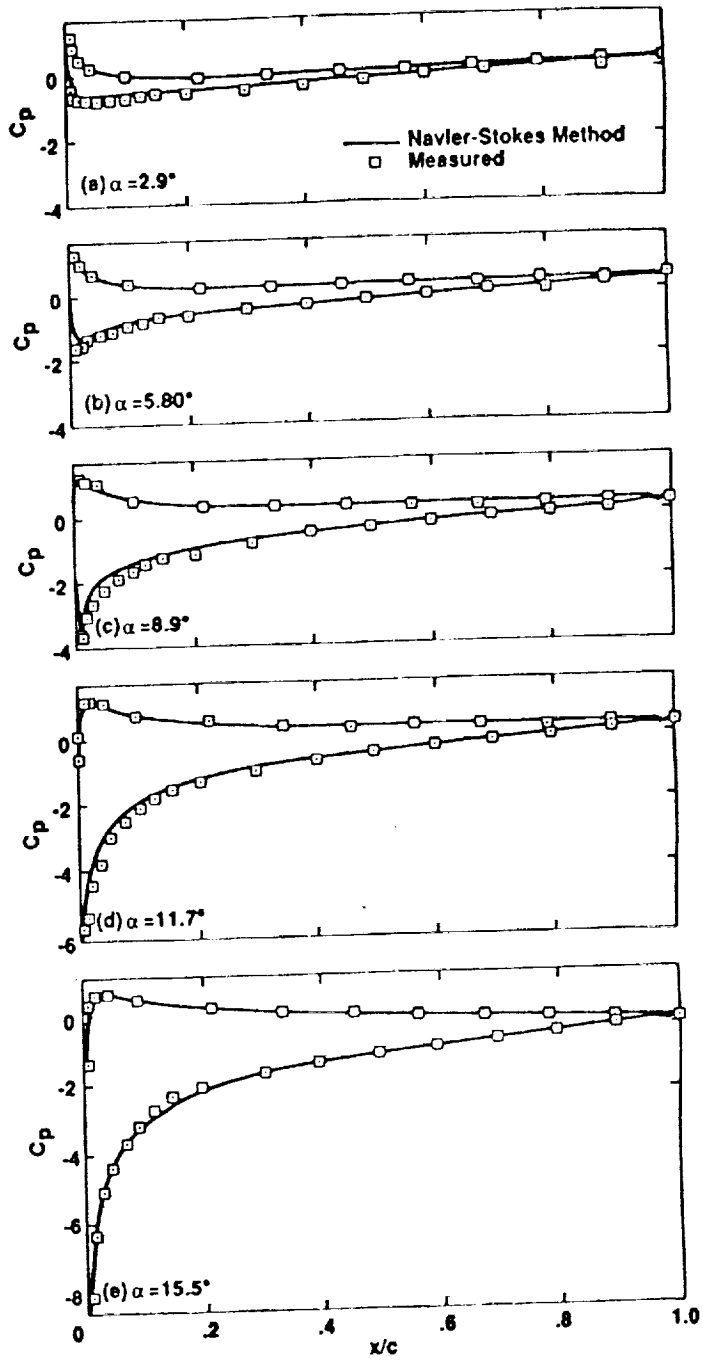

Figure 2 Pressure coefficient distributions predicted by the Navier-Stokes method: ($Re = 2.7 \times 10^6, k = 0.0127$).

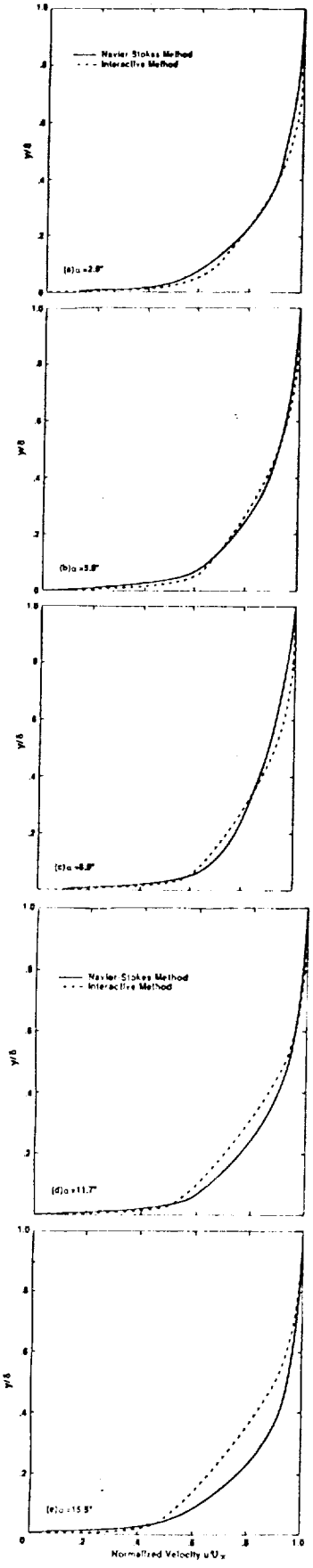

Figure 3 Comparison of the boundary layer profiles computed with both methods, for the 50% chord: ($Re = 2.7 \times 10^6, k = 0.0127$).

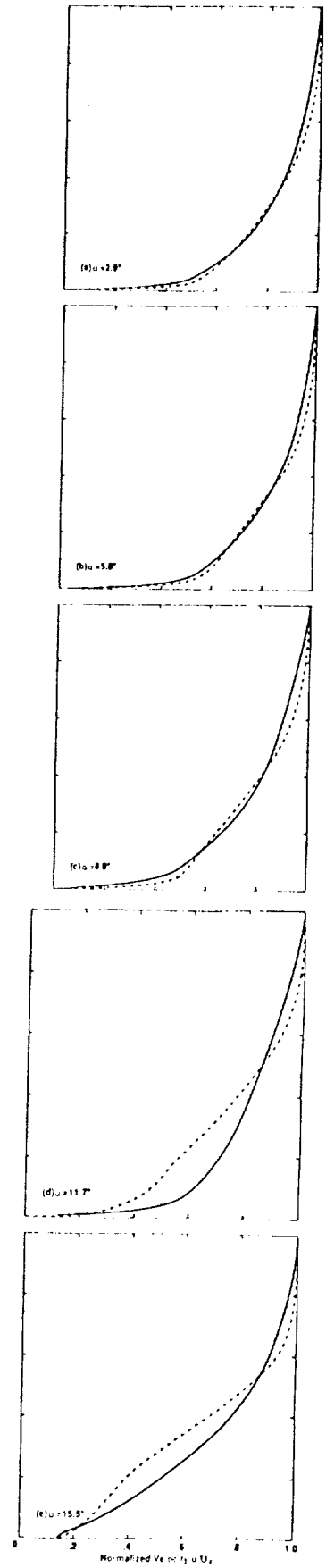

Figure 4 Comparison of the boundary layer profiles computed with both methods, for the 90% chord: ($Re = 2.7 \times 10^6, k = 0.0127$)